two bits of data a 110 Mbits data stream is recovered from the 55 MHz symbol stream.

Experimental results: The measured communication performance of this system is shown in Fig. 4. The data was taken

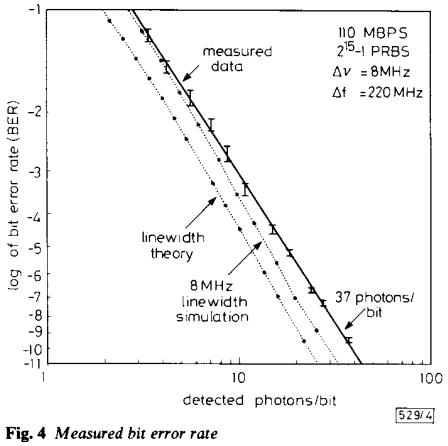

Fig. 4 *Measured bit error rate*

using a $2^{15} - 1$ pseudo-random bit sequence. Also shown are the theoretical curves for a zero linewidth 4-ary FSK system and an estimate of the achievable performance with an 8 MHz linewidth using the techniques in Reference 4 extended to include chip combining and 4-ary modulation. The theoretical limit for ideal zero linewidth 4-ary FSK is 20·7 photon/bit. The measured performance for 4-ary FSK was 37 detected photon/bit at 10^{-9} BER which represents a 2·5 dB loss from ideal. Of the 2·5 dB loss 0·4 dB is due to the use of non-coherent chip combining, 0·75 dB is attributed to linewidth effects predicted in Reference 4, with the remaining 1·35 dB being attributed to residual crosstalk between tones and imperfect modulation and demodulation.

Conclusion: The theoretical quantum limited sensitivity of ideal binary orthogonal FSK using a heterodyne receiver (i.e., no phase tracking) and zero linewidth lasers is 40 photon/bit.[2] This work demonstrates a 4-ary FSK coherent optical communication system using conventional Fabry–Perot lasers that provides a sensitivity of 37 detected photon/bit for a BER of 10^{-9} at 110 Mbits with an 8 MHz IF linewidth. Since this exceeds the sensitivity that could be obtained in an ideal binary system, the sensitivity affored by M-ary signalling is evident despite losses caused by a 7% linewidth, to data rate ratio and to imperfect modulation and demodulation.

Acknowledgment: This work was sponsored by the US Department of the Air Force.

S. B. ALEXANDER
R. BARRY
D. M. CASTAGNOZZI
V. W. S. CHAN
D. M. HODSDON
L. L. JEROMIN
J. E. KAUFMANN
D. M. MATERNA
R. J. PARR
M. L. STEVENS
D. W. WHITE

MIT Lincoln Laboratory
PO Box 73
Lexington, Massachusetts 02173, USA

7th June 1990

References

1 WELFORD, D., and ALEXANDER, S. B.: 'GaAlAs semiconductor diode laser 4-ary frequency shift key modulation at 100 Mbit/s', *Electron. Lett.*, 1985, **21**, (1), pp. 12–13
2 JEROMIN, L. L., and CHAN, V. W. S.: 'M-ary FSK performance for coherent optical communication systems using semiconductor lasers', *IEEE Trans.*, 1986, **COM-34**, (4)
3 LINKE, R. A., and GNAUCK, A. H.: 'High-capacity coherent lightwave systems', *IEEE J. Lightwave Technol.*, 1988, **6**, (11), pp. 1755–1756
4 FOSCHINI, G. J., GREENSTEIN, L. J., and VANNUCCI, G.: 'Noncoherent detection of coherent lightwave signals corrupted by phase noise', *IEEE Trans.*, 1988, **COM-36**, (3), pp. 306–314

SINGLE-QUANTUM-WELL LASER WITH 11·2 DEGREE TRANSVERSE BEAM DIVERGENCE

Indexing terms: Semiconductor lasers, Integrated optics, Optical waveguides

The operation of a single-quantum-well laser, vertically integrated with four passive waveguides to produce a record low beam divergence of 11·2° is reported.

Semiconductor lasers operating in the fundamental transverse mode typically have a large transverse beam divergence ranging from 40° to 60°. A laser with reduced beam divergence will not only improve the light collection efficiency of lenses, but will also relax the requirement of aberration correction. The beam divergence can be reduced by increasing the source size using waveguides with smaller refractive index steps or thinner active layers, one example being the large-optical-cavity laser.[1] However, the increase in source size is limited either by an unacceptable threshold increase or by the onset of higher-order modes. In single quantum well lasers, the reduction in the optical confinement also leads to reduction in the carrier confinement and, in some cases, a runaway increase in the threshold current may occur.[2] Recently, a new approach for reducing the beam divergence using two or three optically and electrically coupled single quantum well lasers has been reported.[3] By monolithic integration of two or three graded index separate confinement (GRINSCH) single quantum well lasers within the minority diffusion length of a *pn* junction, the fundamental mode operation with a 25° far field divergence has been demonstrated. To ensure the fundamental (in phase) mode operation, it is necessary to control the spacing and the relative gains of the wells so that the modal gain of the fundamental mode is the highest. However, it is often difficult to control the gains in individual wells accurately because the carrier densities in the wells are sensitive to the carrier diffusion process and well width variations. In a modified approach, a single-quantum-well laser is vertically integrated with two passive waveguides to produce a beam divergence of 19°.[4] The use of a single gain element simplifies the mode selection and improves the mode stability because the operation is determined solely by the confinement factor within the single gain element, which does not vary with the injection level. In these approaches, a relatively small amount of power in the subordinate waveguides leads to a significant reduction in the beam divergence. Thus beam narrowing is achieved with only a modest threshold penalty.

We report the operation of a single-quantum-well laser vertically integrated with four passive waveguides to achieve a record low beam divergence of 11·2°. While the beam divergence is reduced by a factor of four when compared with a single-quantum-well laser, the threshold current increases by a factor of three. Our analysis shows that it is possible to reduce the threshold current further while maintaining the same low beam divergence.

The laser structure, as shown in Fig. 1, consists of four graded index waveguides symmetrically placed about a GRINSCH single quantum well laser. The centre to centre spacing of the waveguides is 1 μm. The GRINSCH laser consists of a 120 Å thick GaAs single quantum well sandwiched between two 2000 Å thick linearly graded $Al_xGa_{1-x}As$ regions with $0{\cdot}3 < x < 0{\cdot}6$. The four passive waveguides have the same graded index profile except that the GaAs quantum well is replaced by a transparent $Al_{0{\cdot}3}Ga_{0{\cdot}7}As$ layer. The laser

material was grown by atmospheric pressure metalorganic chemical vapour deposition (MOCVD). The MOCVD-grown material was processed into conventional uncoated oxide-stripe lasers 60 μm wide by 600 μm long which were mounted with the junction side down on copper heat sinks.

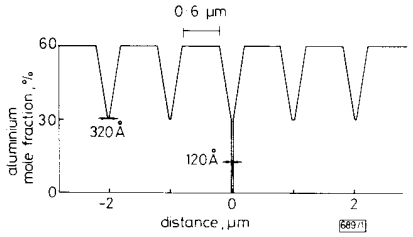

Fig. 1 *Structure of single quantum well laser with four vertical integrated passive waveguides*

The calculated near field and far field light intensity patterns of the eigenmodes for the coupled waveguides are shown in Fig. 2. There are five eigenmodes in these coupled waveguides, each being a linear combination of the eigenmodes of the individual waveguide. The operating mode is the one with the largest confinement factor with the gain medium. The confinement factor can be controlled by the waveguide parameters. Modes B and D are automatically eliminated because their overlapping factors with the gain medium are zero. To determine the parameters for the in-phase mode operation, we have calculated the confinement factors for the in-phase mode A and the mode C having the next highest confinement factor by varying the widths of the valley of the passive waveguides, d, for various waveguide spacings, D. The results are shown in Fig. 3. The in-phase mode has a larger confinement factor for $d < 350$ Å. In this region, the beam divergence,

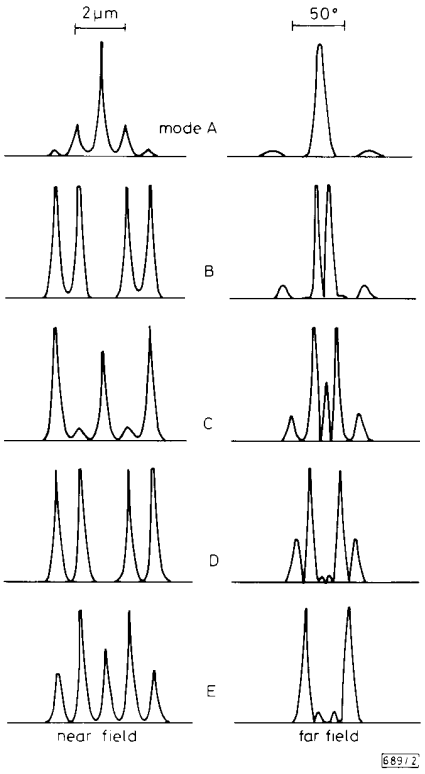

Fig. 2 *Calculated near field and far field patterns for five eigenmodes of the coupled waveguides*

The confinement factors are 1·98%, 0, 0·84%, 0, 0·64% for modes A, B, C, D, and E, respectively

ranging from 14° for $d = 250$ Å to 10° for $d = 350$ Å, is quite insensitive to d. However the power in the side lobes of the far field pattern increases for smaller d. In our experiment, d is chosen to be 320 Å as a compromise between low threshold

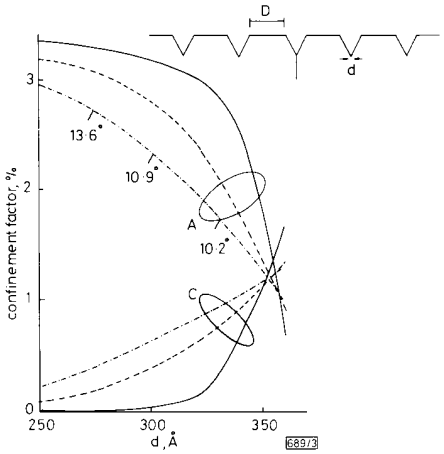

Fig. 3 *Calculated confinement factors of the in-phase mode (A) and mode (C) having the next highest confinement factor, as a function of d, for various values of D*

—·—· $D = 0{\cdot}6\,\mu$m
– – – – $D = 0{\cdot}7\,\mu$m
——— $D = 0{\cdot}9\,\mu$m

The beam divergences at various points on the 0·6 μm curves are labelled

current and higher power in the central lobe. This corresponds to a calculated confinement factor of 1·98% and a beam divergence of 10·8°. For comparison, the GRINSCH single quantum well laser has a confinement factor of 3·8%, threshold current of 120 mA, and beam divergence of 45°.

Typical devices display a room temperature CW threshold current of 370 mA and an external efficiency of 0·3 mW/mA per facet. The threshold current is higher than predicted based on the calculated confinement factor. This is probably because the gain against current relation is already saturated. Our analysis shows that, for a given beam divergence, the confinement factor is larger for larger waveguide spacing. For example, using $d = 350$ Å and $D = 0{\cdot}9\,\mu$m, the beam divergence is still 10·4° and the confinement factor is 2·5%, considerably higher than that of our experimental device.

The measured near field and far field intensity patterns are shown in Fig. 4. The far field pattern exhibits a full-width-half-

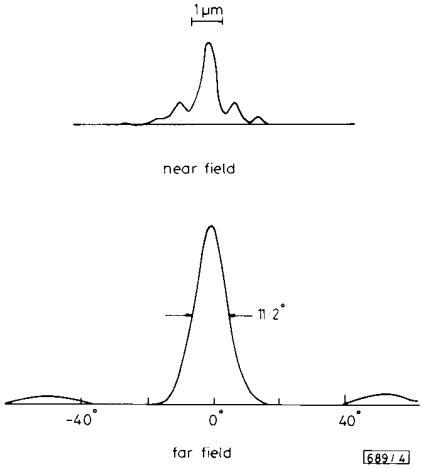

Fig. 4 *Measured near field and far field patterns perpendicular to junction plane at $1{\cdot}5I_{th}$*

maximum divergence of 11·2° compared to 44° in a single-quantum-well laser. The operating mode is stable for currents as high as 1 A. We note that to produce the same beam divergence using a single element GRINSCH single quantum well with reduced refractive index step would result in a serious loss of carrier confinement and a prohibitively high threshold current.

In summary, we have demonstrated the operation of a single-quantum-well laser with four vertically-integrated passive waveguides. The waveguide parameters for the in-phase mode operation have been determined. A record low transverse beam divergence of 11·2° has been achieved.

The authors are indebted to J. DeSanctis, C. Harding, H. Vollmer, R. Soltz, and S. Yellen for valuable technical assistance.

Y. C. CHEN*

Department of Physics and Astronomy
Hunter College of the City University of New York
695 Park Avenue, New York, NY 10021, USA

R. G. WATERS
R. J. DALBY

McDonnell Douglas Electronic Systems Company
Opto-Electronics Center
350 Executive Blvd.
Elmsford, NY 10523, USA

* Also with the Graduate School and University Center, the City University of New York, 33 West 42nd Street, New York, NY 10036, USA

3rd July 1990

References

1 LOCKWOOD, H. F., KRESSEL, H., SOMMERS, H. S., and HAWRYLO, F. Z.: 'An efficient large optical cavity injection laser', *Appl. Phys. Lett.*, 1970, **17**, pp. 499–500

2 REISINGER, A. R., ZORY, P. S., and WATERS, R. G.: 'Cavity length dependence of the threshold behavior in thin quantum well semiconductor lasers', *IEEE J. Quantum Electron.*, 1987, **QE-23**, pp. 993–997

3 WATERS, R. G., EMANUEL, M. A., DALBY, R. J.: 'Integrated quantum-well manifold laser', *J. Appl. Phys.*, 1989, **66**, pp. 961–963

4 CHEN, Y. C., WATERS, R. G., and DALBY, R. J.: 'Single quantum well laser with vertically integrated passive waveguides', *Appl. Phys. Lett.*, 1990, **56**, pp. 1409–1411

CELLULAR AUTOMATA-BASED BUILT-IN SELF-TEST STRUCTURES FOR VLSI SYSTEMS

Indexing terms: Large scale integration, Self-testing devices, Pseudorandom number generation

Some of the fundamental algebraic properties of hybrid additive, null-bounded, cellular automata (HACA) are presented. Simple HACA have been obtained by spatially alternating additive rules 90 and 150 (in Wolfram's notation). The use of such HACA for on-chip pseudorandom test pattern generation is also described. The great advantage of HACA over linear feedback shift registers (LFSR), as their size increases, is the fact that HACA display locality and topological regularity, important attributes for VLSI implementation.

Introduction: Design for testability (DFT) techniques attempt to deal with the inherent complexity of the VLSI testing problem by incorporating testability as a primary element of the design process. Several DFT techniques have been proposed for on-chip circuitry, referred to as built-in self-test (BIST) techniques.[1–4] For cases where an exhaustive test set is prohibitive, a pseudorandomly selected subset of the possible inputs to the circuit under test is used. This requires an on-chip pseudorandom pattern generator. The built-in logic block observation (BILBO) technique[5] employs an LFSR with a maximal cycle length as the pseudorandom sequence generator.

A variation on a BIST technique, based on a distributed pseudorandom number generator derived from 1-D cellular automata (CA), has very recently been presented by Hortensius *et al.*[6] However, there are no formal results leading to rule ordering, necessary for achieving a hybrid additive CA (HACA) with maximal cycle length.

This letter presents some fundamental algebraic properties of HACA with null boundary conditions. The method is based on the characteristic polynomial of the HACA global rule transition matrix.

Definition of HACA: Finite boundary 1-D null-bounded (NB) HACA, with no memory associated beyond the previous clock cycle, are considered in this letter. The total number of possible global states of N-bit HACA is 2^N. HACA evolve in discrete time steps. Null boundary conditions were chosen because they eliminate the need for long feedback paths (with large intrinsic delays), which results from large neighbourhood dependencies. The results in this letter were obtained by spatially alternating the following two specific local rules in Wolfram's notation:[7]

Rule 90:

$$a_i^{(t+1)} = a_{i-1}^{(t)} \oplus a_{i+1}^{(t)} \tag{1}$$

Rule 150:

$$a_i^{(t+1)} = a_{i-1}^{(t)} \oplus a_i^{(t)} \oplus a_{i+1}^{(t)} \tag{2}$$

where $a_i^{(t)}$ and $a_i^{(t+1)}$ are the local states of cell i on clock cycles t and $t+1$, respectively.

Fig. 1 shows one of these 1-D null-bounded HACA with length N (N-bit HACA).

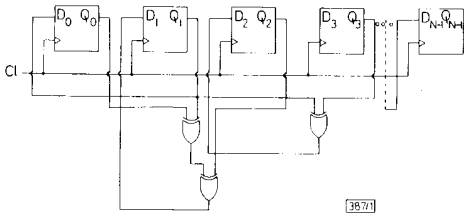

Fig. 1 *1-D N-bit hybrid additive, null-bounded, cellular automaton with null boundary conditions*

Formal analysis of 1-D HACA

Group and semigroup properties of HACA: The global state transformation in one clock cycle may be represented by the following matrix operation:

$$\boldsymbol{S}^{(t+1)} = {}^{H}\boldsymbol{M}_N \boldsymbol{S}^{(t)} \tag{3}$$

where ${}^{H}\boldsymbol{M}_N$ is an $N \times N$ square matrix representing the N-bit HACA global rule for time evolution and $\boldsymbol{S}^{(t)}$ and $\boldsymbol{S}^{(t+1)}$ are $N \times 1$ state column vectors representing the HACA global states on clock cycles t and $(t+1)$, respectively. The global rule transition matrix ${}^{H}\boldsymbol{M}_N$ takes the following form:

$$ {}^{H}\boldsymbol{M}_N = \begin{bmatrix} 0 & 1 & 0 & 0 & 0 & 0 & . & . & . \\ 1 & 1 & 1 & 0 & 0 & 0 & . & . & . \\ 0 & 1 & 0 & 1 & 0 & 0 & . & . & . \\ 0 & 0 & 1 & 1 & 1 & 0 & . & . & . \\ . & . & . & . & . & . & . & . & . \\ . & . & . & . & . & 0 & 1 & 0 & 1 \\ . & . & . & . & . & 0 & 0 & 1 & 1 \end{bmatrix}_{N \times N} \tag{4}$$

HACA may exhibit group or a semigroup algebraic structures. HACA with a global rule transition matrix such that $\det[{}^{H}\boldsymbol{M}_N] = 1$ are referred to as group HACA. The correspond-